Supplemental data

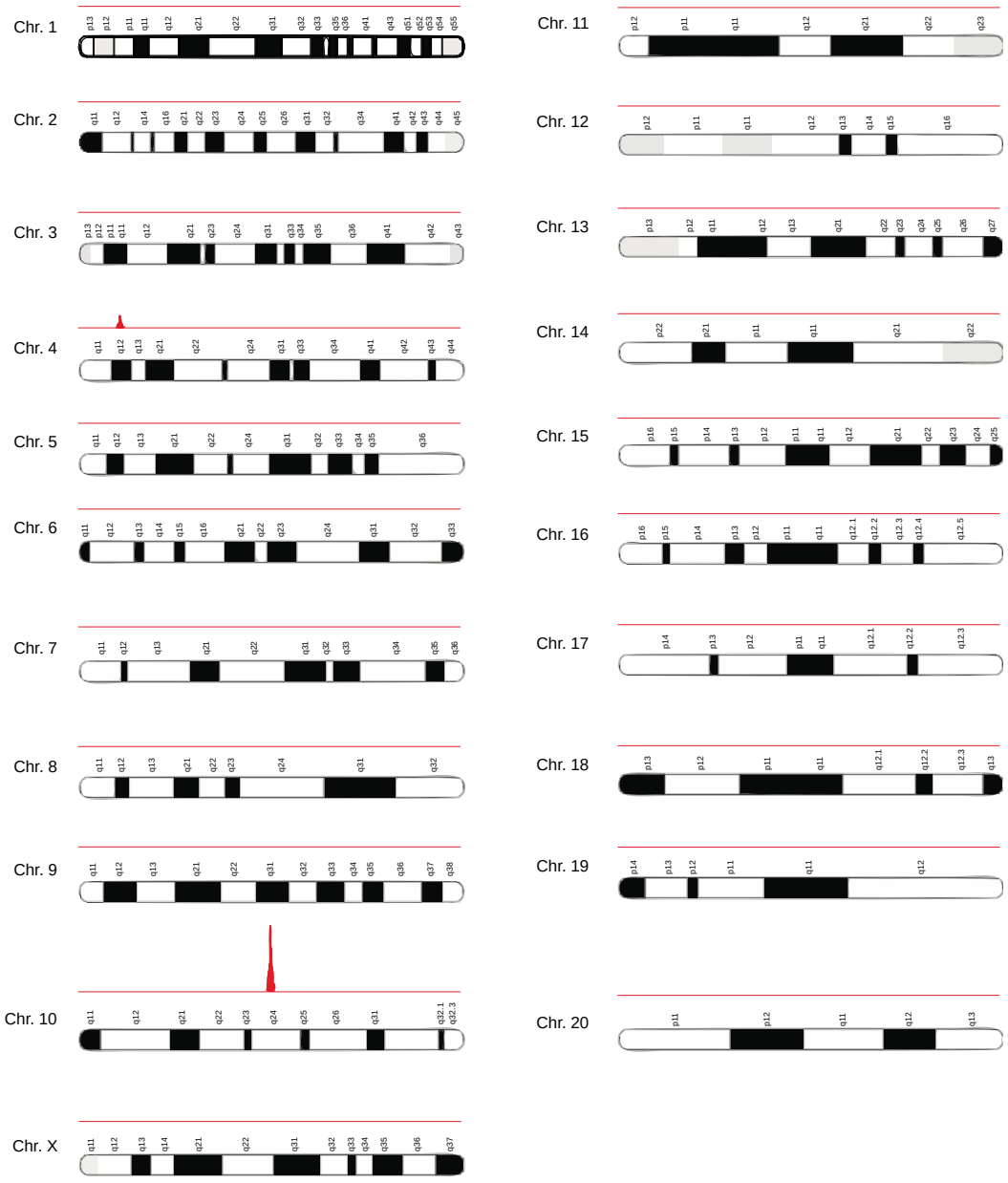

Figure S1. A genome-wide karyotype view of ChIP-seq data from neurons that express PSD95-6ZF-NoED. Related to Figure 4. Cultured hippocampal neurons were infected at 7 DIV with lentiviral particles encoding PSD95-6ZF-NoED. At 12 DIV, chromatin extracts were prepared and immunoprecipitated with an antibody recognizing the HA-tag fused to PSD95-6ZF-NoED (red), or a non-related IgG (as control; not shown). Immunoprecipitated DNA was purified, and used to prepare an Illumina ChIP-seq library to sequence all immunoprecipitated DNA. Chromatin extract not precipitated was used as an input control (not shown). Samples were sequenced using a Miseq personal sequencer, aligned to the rat genome (rn4) using Bowtie2, and analyzed using Strand NGS. Karyotype representation of rat chromosomes 1 to 20, plus the X chromosome, with their approximate loci are shown. Above each chromosome the reads sequenced for the DNA immunoprecipitated with the antibody recognizing the HA-tag of PSD95-6ZF-NoED is depicted in red. Note that only one major peak at the Dlg4/*PSD95* gene promoter sequence (Chr10q24) is detected in the whole genome (see Figure S2A). A smaller peak is observed at the coding sequence (AAGAAGGAGGGGTGCACC) of the rat *Frizzle 1* (*Fzd1*) gene (Chr4q12), which resembles target site for PSD95-6ZF (see Figure S2B for details).

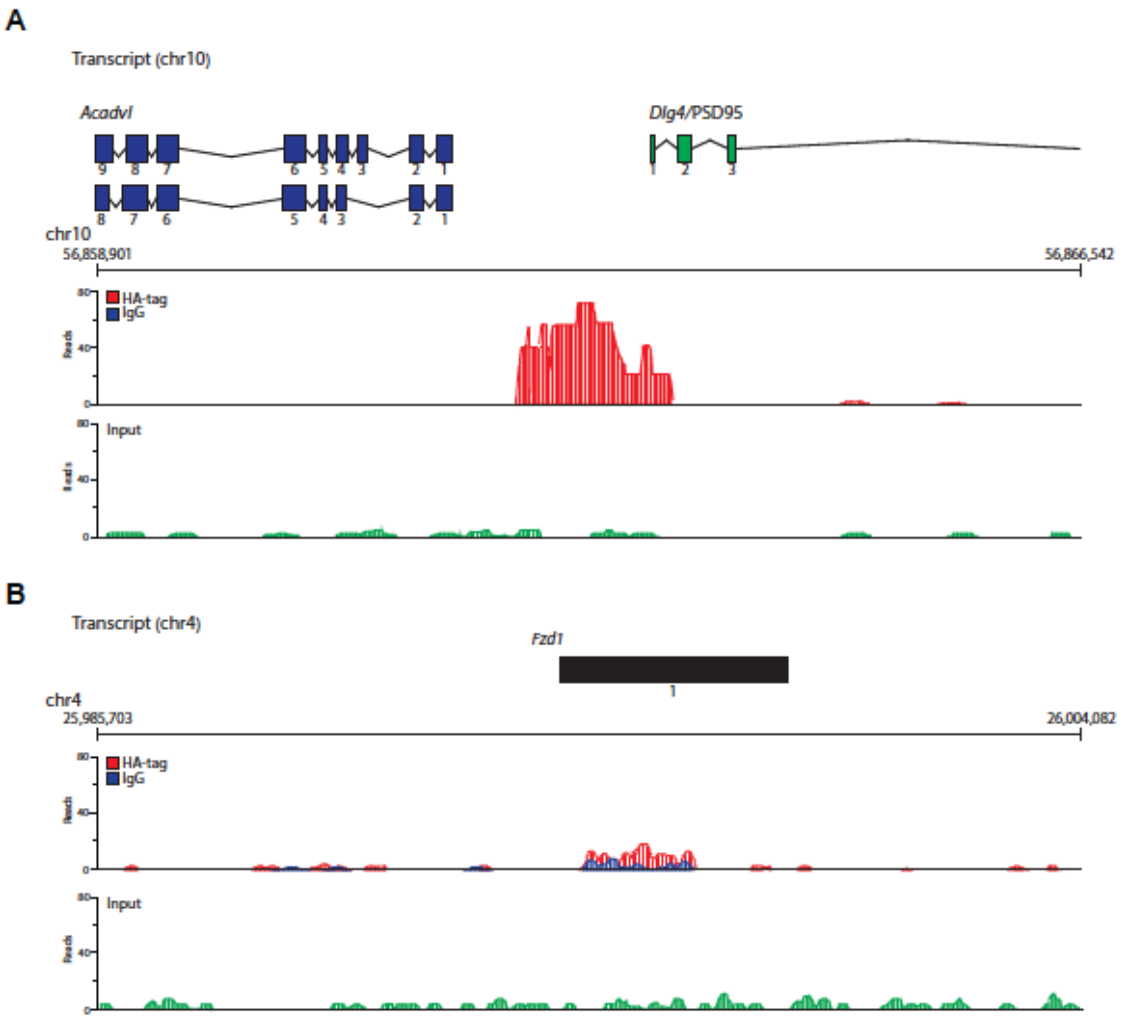

Figure S2. PSD95-6ZF-NoED binds efficiently and specifically to the Dlg4/*PSD95* DNA promoter sequence in hippocampal cells. Related to Figure 4. (**A-B**) Cultured hippocampal neurons at 7 DIV were infected with lentiviral particles encoding PSD95-6ZF-NoED; at 12 DIV, ChIP-seq was performed using an antibody that recognizes the HA-tag fused to PSD95-6ZF-NoED (red peaks). ChIP-seq was also performed using a non-related IgG as control (blue peaks). Immunoprecipitated DNA was purified and used to prepare an Illumina ChIP-seq library to sequence all immunoprecipitated DNA. Chromatin extract that was not precipitated was used as input control (green peaks). Above the graphs of the ChIP-seq data, we show (**A**) a representation of the Dlg4/*PSD95* genomic locus in chromosome 10, where the very long chain acyl-CoA dehydrogenase (*Vlcad*) transcript by the *Acadvl* gene is located in the lagging strand (depicted in blue) and the *Dlg4*/PSD95 transcript is located in the forward strand (depicted in green), and (**B**) a representation of the *Fzd1* genomic locus in chromosome 4, where the *Fzd1* transcript is located in the forward strand (depicted in black).

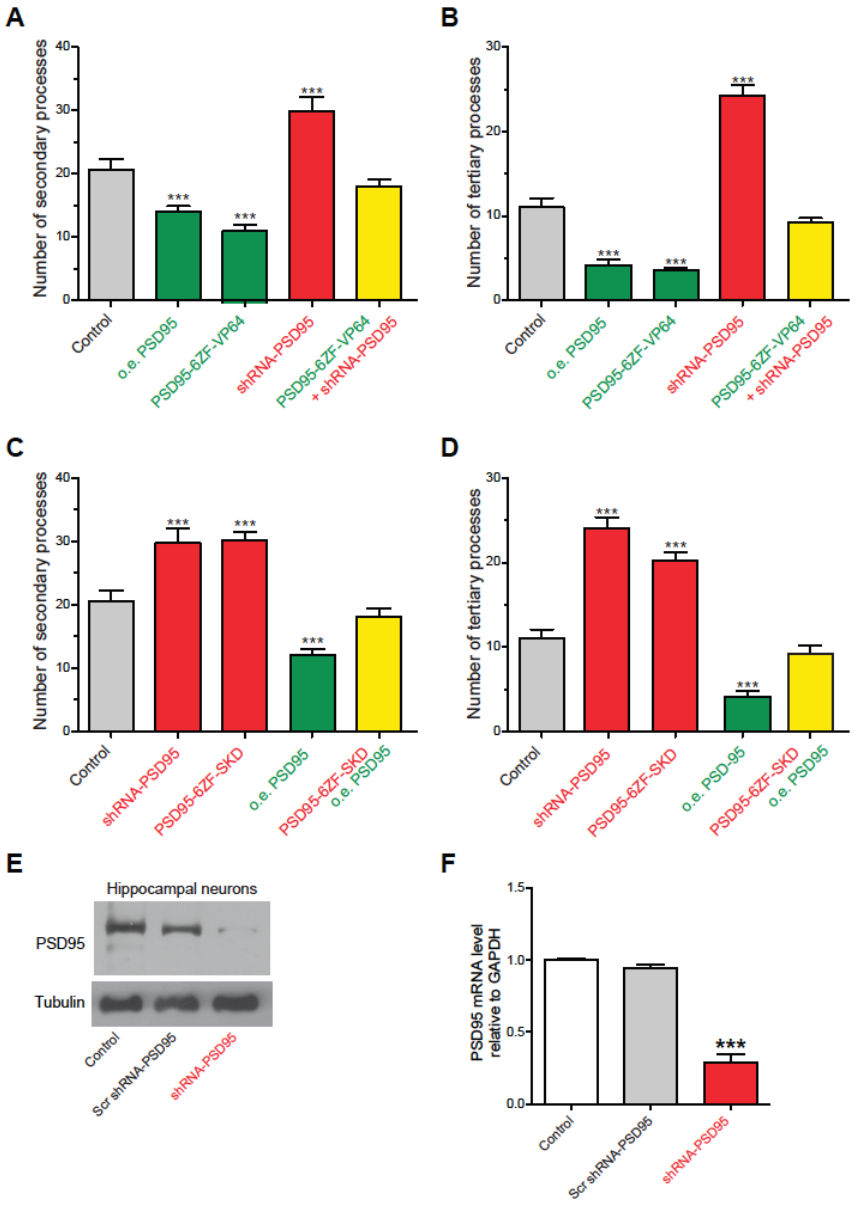

Figure S3. Effects of PSD95-6ZF-VP64 and PSD95-6ZF-SKD on dendritic arborization is rescued by shRNA-PSD95 and by overexpression of Dlg4/*PSD95* cDNA, respectively. Related to Figure 4. Hippocampal neurons (7 DIV) were transfected with pCDH-dual promoter lentiviral vectors, to express GFP alone (Control) or with PSD95-6ZF-VP64 or PSD95-6ZF-SKD. In addition, neurons were transfected with shRNA-PSD95 constructs to knock-down Dlg4/*PSD95*, or transfected with a CMV-driven vector to over-express Dlg4/*PSD95* (o.e.PSD-95); constructs were expressed individually or in combination, as indicated. At 12 DIV, cells were fixed and dendritic arborization quantified. (**A-B**) Graphs show number of (**A**) secondary or (**B**) tertiary processes in cells expressing GFP, or GFP together with o.e.PSD95, PSD95-6ZF-VP64, shRNA-PSD95, or PSD95-6ZF-VP64+shRNA-PSD95. Note that neurons expressing PSD95-6ZF-VP64 and shRNA-PSD95 display dendritic arborization as in control neurons. (**C-D**) Graph show number of (**C**) secondary or (**D**) tertiary processes in cells expressing GFP, or GFP together with shRNA-PSD95, PSD95-6ZF-SKD, or PSD95-6ZF-SKD+o.e.PSD95. Note that dendritic architecture of neurons expressing PSD95-6ZF-SKD+o.e.PSD95 is similar to that of control neurons. At least 24 neurons from 3 independent experiments were analyzed for each condition. Bars represent means ± S.E.M.; statistical analysis was performed using ANOVA. ***P<0.001, relative to control. (**E-F**) Hippocampal cultures were transfected with constructs harboring GFP (GFP), GFP plus scrambled shRNA (scr shRNA), or shRNA against Dlg4/*PSD95* (shRNA-PSD95); 2-3 days later, total (**E**) protein or (**F**) RNA extracts were obtained. PSD95 protein levels determined by western blot; tubulin was protein loading control. Dlg4/*PSD95* mRNA levels measured by qRT-PCR were normalized against GAPDH mRNA. Bars represent means ± S.E.M.; statistical analysis was performed using ANOVA. ***P<0.001, relative to control.

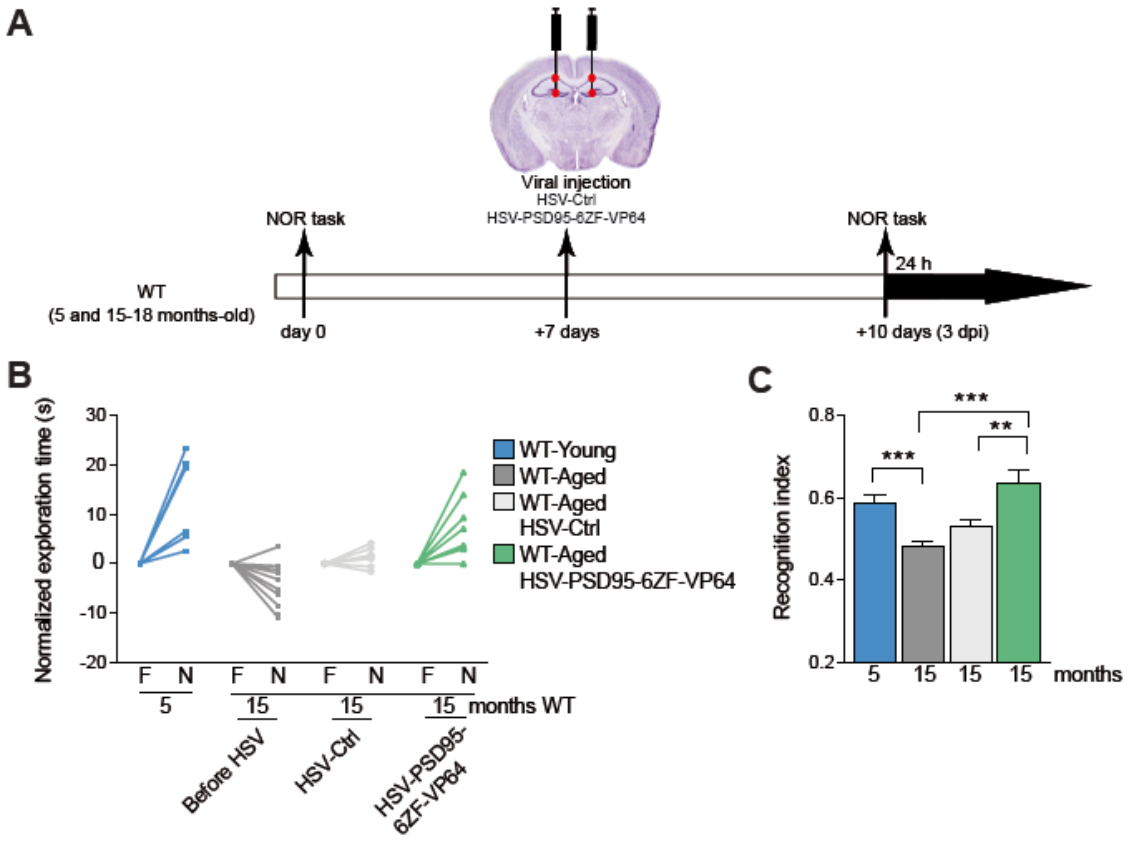

Figure S4. HSV-PSD95-6ZF-VP64 treatment reverts NOR impairment in aged mice. (**A**) Scheme of experiment. Wild-type young (5 mo) and aged mice (15-18 mo) performed the novel object recognition (NOR) task before (7 days) and after (3 days) injections of HSV-Ctrl or HSV-PSD95-6ZF-VP64 into DG, CA1 and CA3 (indicated by red dots). (**B**) Mice were exposed to two similar objects and 24 hr later re-exposed for 10 min to the testing area now containing a novel object. Normalized exploration time shows time spent (in sec) of individual mice on the familiar (F) *versus* novel (N) object. (**C**) Recognition index, corresponding to the time spent to explore the novel object / total time spent to explore both objects. An index of 0.5 indicates that mice do not discriminate between a novel and familiar object. Values represent Mean ± S.E.M. from ≥7 mice per condition. Statistical analysis was performed using one-way ANOVA followed by Bonferroni *post hoc* test. **p<0.01, ***p<0.001.

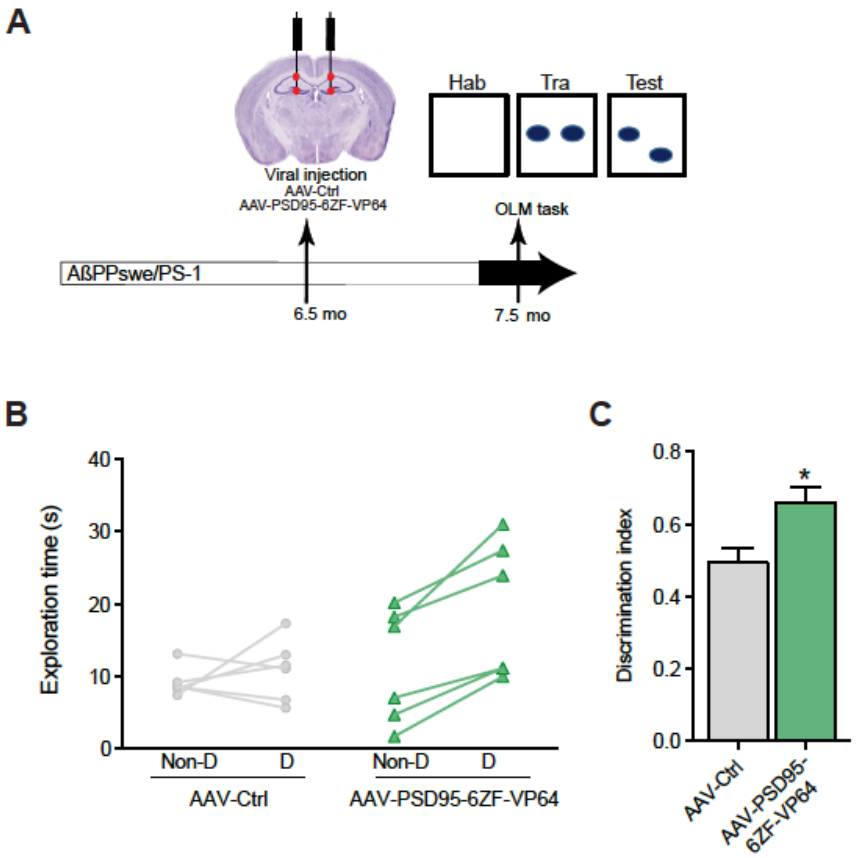

Figure S5. AAV-PSD95-6ZF-VP64 treatment improves object location memory (OLM) performance in AβPPswe/PS-1 mice. Related to Figure 6. (**A**) Scheme of experiment. AAV-PHP.B carrying GFP alone (AAV-Ctrl) or GFP plus PSD95-6ZF-VP64 (AAV-PSD95-6ZF-VP64) were generated and injected in 6.5 mo AβPPswe/PS-1 mice into the hippocampus (CA1 and DG, as indicated by red dots). The single-trail OLM task was tested four weeks after AAV injections on 7.5 mo mice. In this test, mice were exposed to two similar objects ("training; Tra") and 24 hr later tested ("Test") re-exposed for 10 min to the testing area now with one object displaced. (**B**) Total exploration time (in sec) of individual AAV-Ctrl- or AAV-PSD95-6ZF-VP64-treated mice on the non-displaced (non-D) *versus* displaced (D) object. (**C**) Discrimination index, corresponding to the time spent to explore the displaced object/total time spent to explore both objects. A recognition index of 0.5 indicates that mice do not discriminate between the displaced object and non-displaced object. Value represent means ± S.E.M. Statistical analysis was performed Student´s *t*-test. *p<0.05.

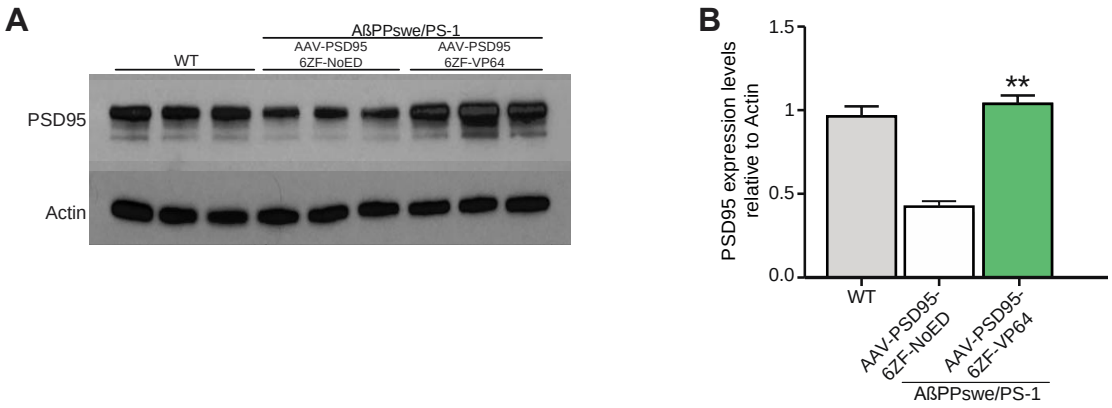

Figure S6. Infection of AβPPswe/PS-1 mice hippocampi with AAV-PSD95-6ZF-VP64 significantly increases PSD95 expression, reaching levels comparable to age-matched wild-type mice. 6.5 mo AβPPswe/PS-1 mice were stereotaxically injected into CA1 and DG with AAV-PSD95-6ZF-VP64 or AAV-PSD95-ZFP-NoED (no effector domain) as control. At 12 mo, whole homogenates were prepared from the AβPPswe/PS-1 mice as well as from untreated age-matched wild-type mice (WT). (**A**) Western blot showing total expression of PSD95 from individual hippocampi. Actin was used as loading control. (**B**) Quantification of the changes in PSD95 expression relative to actin. One-way ANOVA followed by Bonferroni *post hoc* test revealed significant differences between AβPPswe/PS-1 AAV-Ctrl and AAV-PSD95-6ZF-VP64 treated animals (**$p<0.01$). A total number of 3 WT, 3 AβPPswe/PS-1 AAV-Ctrl, and 6 AβPPswe/PS-1 AAV-PSD95-6ZF-VP64 hippocampi were used for quantifications.

Supplemental Experimental Procedures

Animals. All protocols involving rodents were carried out according to NIH guidelines and ARRIVE guidelines (Kilkenny *et al.,* 2010), and were approved by the Ethical and Bio-security Committees of Universidad Andrés Bello. Female pregnant Sprague-Dawley rats were deeply anesthetized with CO_2, and hippocampi were isolated at embryonic day E 18. Additionally, hippocampi from rats were isolated at postnatal day (P) 10, P30, or >P90. Wild-type C57B6/SJ (000664; Jackson laboratory), AβPPswe/PS-1 (004462; Jackson laboratory) and their wild-type background animals B6C3F1/J (100010; Jackson laboratory) were anesthetized with ketamine plus xylazine, and hence stereotaxically injected with HSV or AAV particles into the hippocampus (CA1, CA3 and DG) (see section stereotaxic injections).

Cell cultures, transfections and infections. Primary cultures of rat hippocampal neurons were prepared as described (Henriquez *et al.,* 2013; Bustos *et al.,* 2014). Briefly, hippocampi of E18 fetuses were excised, minced, and re-suspended by mechanical agitation. Cells were counted and plated on freshly prepared poly-L-lysine-coated 24 or 6-well plates: 20,000 cells/ml for immunofluorescence and $1x10^6$ cells/well for all other experiments. Plating media comprised DMEM (Hyclone, SH30081.02) supplemented with 10% horse serum (Hyclone, SH30074.03), and 100 U/ml penicillin/streptomycin (Life Technologies, 15070-063). Next day, the plating medium was replaced by growth medium - MEM (Life Technologies 21103-049) supplemented with B27 (Life Technologies, 17504044), 2 mM L-glutamine (Life Technologies, 25030- 081), 100 U/ml penicillin/streptomycin. On day 2, hippocampal neurons were treated with 2 µM cytosine arabinoside (AraC) for 24 hr. Media was replaced every 3 days, and cultures were maintained until 21 DIV. Hippocampal neurons were transfected according to a CaPO4 transfection protocol (adapted to reduce cell toxicity) (Sepulveda *et al.,* 2010; Bustos *et al.,* 2014), or were infected by viral particles containing diverse PSD95-ZFP constructs (see below). Mouse N2a cells and HEK293FT cells were grown in DMEM medium (Hyclone), supplemented with 10% Fetal Calf Serum (FCS, Hyclone) or Fetal Bovine Serum (FBS, Hyclone), 100 U/ml penicillin, and 100 µg/ml streptomycin. N2a cells were seeded in 100 mm plates, and differentiated by serum starvation (0.1% FCS). Both N2a and HEK293FT cells were maintained at 37°C in 5% CO2 atmosphere, and were infected by viral particles containing diverse PSD95-6ZF constructs. To infect cultures of primary hippocampal neurons, all constructs were first subcloned into a lentiviral bicistronic pCDH vector expressing cop-GFP (System Biosciences).

Chromatin immunoprecipitation (ChIP) assays. ChIP assays were performed on hippocampal tissue as described (Henriquez *et al.,* 2013). Isolated hippocampal tissue from E18, P10, P30 or >P90 Sprague Dawley rats were cross-linked with 1% PFA in phosphate buffer saline (PBS), and were incubated at room temperature for 30 min with gentle agitation. The tissue was washed three times with cold PBS. For ChIP against chromatin-modifying enzymes, we used double cross-linking with EGS (Ethylene glycol-bis(succinic acid N-hydroxysuccinimide ester; E3257, Sigma): the PFA cross-linked cells were incubated with EGS for 1 hr at room temperature with gentle agitation, washed three times with cold PBS, and resuspended in 1 ml of cell lysis buffer (CLB; 5 mM HEPES, pH 8.0, 85 mM KCl, Triton X-100 and proteinase inhibitors). Cells were homogenized with a Dounce homogenizer (150 times using a tight pestle). Tissue extract was collected by centrifugation at 3000xg for 5 min, and was resuspended in 1ml of CLB. Cells were incubated with 10 µg of RNase-Free DNase on ice for 1 hr. Extracts were centrifuged at 3000×g for 5 min at 4ºC, the supernatant was discarded and pelleted nuclei were resuspended in 600 µl sonication buffer (50 mM HEPES, pH 7.9, 140 mM NaCl, 1 mM EDTA, 1% Triton X-100, 0.1% deoxycholate acid, 0.1% SDS, and a mixture of proteinase inhibitors). Chromatin was sheared in a water bath sonicator Bioruptor (Diagenode Inc., Denville, NJ, USA) to obtain fragments of 500 bp or smaller. Chromatin size was confirmed by electrophoretic analysis. Cross-linked extracts (2 A260 units) were resuspended in sonication buffer to a final volume of 500 µl; samples were pre-cleared by incubating with 2-4 µg of normal IgG and 50 µl of protein A/G-agarose beads (Santa Cruz Biotechnology) for 1 hr at 4°C with agitation. Chromatin was centrifuged at 4,000×g for 5 min, the supernatant was collected, and was immunoprecipitated with specific antibodies (see list of antibodies below) for 12-16 hr at 4°C. The immunocomplexes were recovered with addition of 50 µl of protein A or G-agarose beads, followed by incubation for 1 hr at 4°C with gentle agitation. Immunoprecipitated complexes were washed once with sonication buffer, twice with LiCl buffer (100 mM Tris-HCl, pH 8.0, 500 mM LiCl, 0.1% Nonidet P40, and 0.1% deoxycholic acid), and once with Tris-EDTA (TE) buffer at pH 8.0 (2 mM EDTA and 50 mM Tris-HCl, pH 8.0), each time for 5 min at 4°C; followed by centrifugation at 4000×g for 5 min. The protein-DNA complexes were eluted by incubation with 100 µl of elution buffer (50 mM NaHCO3 and 1% SDS) for 15 min at 65°C. Extracts were centrifuged at 10,000×g for 5 min, and the supernatant was collected

and incubated for 12-16 h at 65°C to reverse the cross-linking. Proteins were digested with 100 µg/ml of proteinase K for 2 h at 50°C, and DNA was recovered by phenol/chloroform extraction and ethanol precipitation using glycogen (20 µg/ml) as a precipitation carrier. The qPCR primers used to evaluate the rat *Dlg4*/PSD95 gene promoter region were: Fw -33 (GGA GGG GTG AGA ACC CAC CGA) and Rev +118 (CTC CCC CTC CCC ACT GCT CC). The primers for the rat *Dlg4*/PSD95 coding region (between exons 10 and 12) were: Fw: CAC ATT GGA AAG GGT GAG CA, and Rev: AAA GGG AAC GGG ACA GGA TT. As a positive control for repression marks, we made use of the *Runx2* P1 promoter region Fw: GTG GTA GGC AGT CCC ACT TT Rev: TGT TTG TGA GGC GAA TGA AG. The following antibodies were used for ChIP assays: total H3 histone (ab1791, Abcam), total acetylation H3 (06-599, Millipore), H3K9Ac (06-942, Millipore), H3K27Ac (ab4729, Abcam), H3K4me3 (ab1012, Abcam), H3K9me2 (07-441, Millipore), H3K9me3 (ab8898, abcam), CBP (sc-369, Santa Cruz Biotechnology), p300 (554215, BD Pharmingen), GCN5 (sc-20698, Santa Cruz Biotechnology), Wdr5 (ab56919, Abcam), G9a (PP-A8620A-00, PPMX), Suv39H1 (ab12405, Abcam), or Ha-tag (ab9110, Abcam).

ChIP-sequencing. Precipitated DNA obtained from ChIP experiments was subjected to sonication by Bioruptor (90 min at low intensity, 30 seconds ON/OFF), to obtain small-sized DNA fragments (100-300bp). DNA size was analyzed by a Fragment Analyzer (Advanced Analytical, USA). Libraries were constructed with use of a TruSeq DNA LT Sample Prep Kit (Illumina, USA) and quantified using KAPA library quantification kit (Illumina, USA); 12pM of pooled libraries were loaded into MiSeq Reagent Kit v2 (Illumina, USA), and sequenced using pair-end reads for 300 cycles on a Miseq desktop sequencer (Illumina, USA). Sequences were aligned with Bowtie2 (Langmead and Salzberg, 2012) against the latest Rattus norvegicus genome (rn4) and peak detection was performed using Avadis NGS software (Strand, USA).

Bisulfite sequencing. Sequencing of methylated DNA sequences was performed as described (Huisman *et al.*, 2013; Falahi *et al.*, 2013). Methylation status of 12 CpGs in the *Dlg4*/PSD95 DNA promoter sequence was determined by bisulfite sequencing. Genomic DNA was obtained from hippocampal tissue, using the Quick-gDNA kit (Zymo Research, USA), following manufacturer's instructions. Genomic DNA was bisulfite-converted with the EZ-DNA-Methylation Gold kit (Zymo Research, USA). PCR was used to amplify the 258 bp *Dlg4*/PSD95 gene region encompassing the 12 CpGs with the following primers. Forward: 5'AGTGAAGGAGTTAATATTGTTAAGGTA3'; Reverse: 5'CTAACAACCCCRAAATTCT3'. The PCR product obtained was cloned into pCR2.1 vector (Life technologies, USA), and sequenced with M13 reverse primer 5'CAGGAAACAGCTATGAC3'. Analysis was conducted by bisulfite sequencing DNA methylation analysis (http://biochem.jacobs-university.de/BDPC/BISMA).

Reverse transcriptase and quantitative real-time PCR (qRT-PCR) assays. qRT-PCR to detect *Dlg4*/PSD95 mRNA levels was performed as described (Henriquez *et al.*, 2013; Bustos *et al.*, 2014). Total RNA was extracted with TRIzol (Life Technologies), according to the manufacturer's protocol. Equal amounts of each sample (1-2 µg) were used for reverse transcription. qPCR was performed using Brilliant II SYBR® Green QPCR Master Mix (Agilent technologies, 600828). Data are presented as relative mRNA levels for the gene of interest, normalized to *GAPDH* mRNA levels. Primers used were: *PSD95* Fw: GCCCTGTTTGATTACGACAA, Rv: CTCATAGCTCAGAACCGAGT; *GAPDH* Fw: CATGGCCTTCCGTGTTCCTA, Rv: CCTGCTTCACCACCTTCTTGAT.

Western blots. PSD95 protein levels were detected via western blot, as previously described (Henriquez *et al.*, 2013; Bustos *et al.*, 2014). Whole cell lysates were prepared in a buffer containing 50 mM Tris HCL pH 7.4, 150 mM NaCl, 0.1% SDS, 1% NP-40, 0.5% sodium deoxycholate, plus proteinase and phosphatase inhibitors. Samples (10-20 µg) were run on a 10% SDS-PAGE gel and transferred to a nitrocellulose membrane, which was blocked with 5% milk in TBS/Tween20, and incubated overnight at 4°C with primary antibodies against PSD95 (1:10000, UC Davis/NIH NeuroMab Facility, 75-028). As loading controls, antibodies against GAPDH (1:5000, Abcam, ab9485), N-Cadherin (1:1000, Santa Cruz Biotechnology, H-63), tubulin (1:1000, Santa Cruz Biotechnology, sc8035), or actin (1:5000, Abcam, ab8226) were used. Membranes were washed in TBS/Tween20, incubated with an HRP-conjugated secondary antibody (1:5000, Santa Cruz Biotechnology) for 1 hour at RT, washed, incubated with ECL solution (Perkin Elmer) for 1 min, and exposed for 1-3 min on Biorad films or developed using a C-DiGit Blot Scanner (LI-COR).

Synaptic membrane preparation. Adult mice were decapitated and hippocampi and prefrontal cortices were quickly dissected on ice and placed in homogenization buffer (0.32 M sucrose, 0.5 mM EGTA, 5 mM HEPES pH 7.4) supplemented with a mixture of protease inhibitors (PI, catalog number 14583900 Roche Diagnostics GmbH, Indianapolis, USA). Subcellular fractionation was performed with modifications of Wyneken *et al.* (2001), adapted to work with small tissue quantities (120 mg/sample). The tissue homogenate were

centrifuged for 20 min at 12,000 g to re-suspend the pellet in PBS plus PI and repeat centrifugation for 20 min at 12,000 g. The pellet (P2 or crude membrane fraction) was re-suspended in 1mM Tris/HCl pH 8.1 to perform a hypo-osmotic shock to release intracellular organelles. The subsequent pellet, obtained after centrifugation for 1 hour at 100,000 g, was re-suspended in 5mM Tris/HCl/0.32 M sucrose, pH 8.1 and loaded on a 1M/1.2M sucrose step gradient to centrifuge for 1 hour at 100,000 g. Synaptic membranes were collected from the 1/1.2M interphase, while the pellet (mitochondria and cell debris) was discarded. The synaptic membrane fraction was diluted 1:3 with Tris/HCl pH 8.1 and centrifuged at 100,000 g for 1 h to obtain the pellet, i.e. synaptic membranes, that were re-suspended in 100 µL of 50 mM HEPES, pH 7.4. Protein concentrations were determined using the BCA assay (Pierce, Rockford, IL).

Engineering of PSD95-6ZF-fusion constructs. We generated a C_2H_2 DNA-binding domain with 6 zinc fingers targeting 6 DNA triplets: each finger is composed of 30 amino acids that fold into a ββα configuration, coordinating one Zn^+ atom using two cysteines (C) and two histidines (H) residues to contact 3-4 bp DNAs. To design PSD95-6ZF DNA-binding domain, the sequence of the TSS gene region of *PSD95/DLG4* screened for 18 contiguous basepairs that showed putative high affinity to established zinc fingers (http://www.zincfingertools.org/) (Mandell and Barbas, 2006). The following zinc fingers with high affinity and target site specificity were selected to target the *Dlg4*/PSD95 gene promoter DNA sequence: 3' - GAA – TGA – GGG – GAG - GGG – AGG -5´. The resulting amino acid sequence of the complete PSD95-6ZF is as follows: LEPGEKPYKCPECGKSFS**QSSNLVR**HQRTHTGEKPYKCPECGKSFS**QAGHLAS**HQRTHTGEKPYKC PECGKSFS**RSDKLVR**HQRTHTGEKPYKCPECGKSFS**RSDNLVR**HQRTHTGEKPYKCPECGKSFS**RSD KLVR**HQRTHTGEKPYKCPECGKSFS**RSDHLTN**HQRTHTGKKTS. In blue are highlighted the helixes that interact with the DNA sequence. PSD95-6ZF was fused to a HA-tag and a nuclear localization sequence. For expression, the construct was subcloned into a pMX-IRES-GFP retroviral vector containing the transcription effector domains VP64, SKD, and the sequence of catalytic domains of the histone methyltransferase enzymes G9a and Suvdel76 (Falahi *et al.*, 2013). To infect primary hippocampal neurons, all PSD95-6ZF-fusion constructs were subcloned into a lentiviral bicistronic pCDH vector expressing cop-GFP (System Biosciences) and lentiviral particles produced. To infect neurons *in vivo*, PSD95-6ZF-fusion constructs were subcloned into p1005 HSV vector, or into AAV vectors to produce viral particles. All vectors used for HSV, AAV, retroviral and lentiviral production coded for the expression of GFP using an independent promoter.

Viral vectors and delivery. To infect N2a cells, PSD95-6ZF was subcloned into the pMX-IRES-GFP retroviral plasmid to produce retroviral vectors (1×10^6 pfu/ml) as described (Beltran *et al.*, 2007). For transductions of hippocampal cultures, lentiviral vectors (1×10^7 TU/ml) were prepared as described (Henriquez *et al.*, 2013). Briefly, to produce retroviral and lentiviral vectors, HEK293FT cells were grown in 100 mm culture plates to 80-90% confluence; Lipofectamine 2000 reagent (Life Technologies; following manufacturer's instructions) or CaPO4 was used to transfect cells with the pMX or pCDH plasmid containing the PSD95-6ZFP and effector domains (VP64, SKD, G9a, or Suvdel76), together with viral packaging plasmids (containing cDNA encoding gag-pol and the vesicular stomatitis virus G protein). Empty pMX or pCDH plasmids (GFP only), and backbones with only PSD95-6ZFPs, were used as control. N2a cells and hippocampal neurons were plated in 24 or 6-wells plates, infected with the supernatant of HEK293FT cells, and collected 48 hr post-transfection for N2a cells and 7 days after infection for neurons. For *in vivo* transductions, we used HSVs because the expression is robust and rapid (i.e., initiated 2-3 hr post-injection); also, unlike many viruses, HSVs are naturally neurotropic (Neve *et al.*, 2005). Recombinant p1005 HSV viruses (~1×10^8 infectious units/ml) expressing eGFP alone (driven by a CMV promoter), or together with PSD95-6ZFP fusion constructs (driven by an IE 4/5 promoter), were generated as described (Neve *et al.*, 2005) by the viral core facility at MIT (now the Gene Delivery Technology Core at Massachusetts General Hospital, Cambridge). AAV vectors were used to achieve widespread transduction and stable transgene expression in the hippocampus. AAV vectors were produced with the PHP.B capsid (Deverman *et al.*, 2016). The following AAV viral vectors were generated: AAV vectors encoding PSD95-6ZF-VP64 were driven by a CBA promoter and carried an IRES-GFP cassette (1.8×10^{12} vg/ml), and AAV vectors expressing GFP alone were driven by a CBA promoter (6.5×10^{12} vg/ml). Briefly, AAV-PHP.B vectors were produced by triple transient transfection of HEK-293 cells followed by purification using iodixanol gradient centrifugation. The AAV-PHP.B capsid gene was synthesized based on the published sequence (Genbank KU056473; Deverman *et al*, 2016) and cloned in a trans-complementing plasmid carrying the AAV2 Rep gene as previously described (Broekman *et al*, 2006; PMID: 16414198). Iodixanol was removed from vector fractions using Zeba spin desalting columns (ThermoFisher Scientific, USA). AAV vectors were concentrated using 100K centrifugal devices (EMD Millipore, USA) using phosphate buffered saline (PBS). Titers were determined by quantitative real-time PCR using primers and probe specific for the bovine growth hormone polyadenylation signal as described (Broekman *et al*, 2006).

Stereotaxic injection. Bilateral hippocampal stereotaxic injections of viral particles were performed as previously described for HSV particles (Bustos *et al.,* 2017; Ampuero *et al.,* 2017). Briefly, adult mice were anesthetized with saline (5 µl saline/gram body weight) containing 170 mg/kg ketamine plus 17 mg/kg xylazine. For spine morphology analysis, 1.0 µl of 10% diluted HSV (0.1 µl of ~1 x 10^8 infectious units/ml + 0.9 µl HEPES) was injected into DG, with the following coordinates: ± 1.5 mm lateral; -2 mm anteroposterior; -2.3 mm ventral from bregma (Tashiro *et al.,* 2006). For hippocampal electrophysiology recordings, 1.0 µl of µl µl 25% diluted HSV (0.25 µl of ~1 x 10^8 infectious units/ml + 0.75 µl HEPES) was injected into DG (± 1.5 mm lateral; -2 mm anteroposterior; -2.3 mm ventral from bregma), CA1 (± 1.5 mm lateral; -2 mm anteroposterior; -1.3 mm ventral from bregma) and CA3 (± 2.5 mm lateral; -2 mm anteroposterior; -1.5 mm ventral from bregma (Tashiro *et al.,* 2006). For behavioral studies, HSVs (0.5 µl 25% diluted) or AAVs (0.5 µl undiluted) were bilaterally injected into CA1 and DG using the above coordinates.

Spine morphology. For dendrite selection and image acquisition, for each experimental condition 8-10 granular neurons of the dentate gyrus (DG) were selected. Secondary dendrite shafts (≥ 30 µm) were chosen by the following characteristics: high signal-to-noise ratio for GFP, and relative isolation from neighboring GFP infected cells. Low-magnification images were acquired with a Leica LSI Macro-Zoom confocal laser scanning microscope with a 5x air objective (NA = 0.12) plus optical zoom 1.7x, excitation with solid state laser at 488 nm, and spectral detection. 8-Bit TIFF images of 1024 × 1024 pixels were acquired with 0.1 µm between z-sections, and then projected into one 2D image (maximum intensity projection). To obtain a broad field of acquisition, the mosaic function in LAS-AF software (Leica Microsystems) was used. Microscope settings were adjusted in order to optimize brightness and contrast in the samples. To analyze and classify dendritic spines, high-magnification images were acquired with an UltraView RS spinning disk microscope (Perkin-Elmer) with a 100x oil objective (NA = 1.3, C-Apochromat), excitation with a 488 nm diode laser (Omicron), a 12-bit CCD camera (Hamamatsu ORCA-ER), and Volocity 4.2 software (Improvision). 8-Bit TIFF images of 1,344 × 1,024 pixels were acquired with 41.5 × 41.5 nm pixel size and 100 nm between z-sections. 70-100 z-sections were acquired, depending on the dendrite positioning through the sample. For the segmentation of dendrite shafts and dendritic spines, high-magnification images were deconvolved with Huygens Scripting software (Scientific Volume Imaging BV) to reduce blurring and noise. From the secondary dendrite shafts, segments of 30 µm lengths were selected to segment dendrite shafts and spines. To this end, we used the interactive supervised segmentation tool (support vector machine) from the Ilastik software (version 0.5.06). Using the 3D image orthogonal viewer, we manually marked dendrites and their spines, and separated these from the background. Support vector machine was trained with 6 images (2 from each condition), and applied for the segmentation of shafts and spines in the rest of the images. Since the microscope point spread function can fuse neighboring spines into a single object, the segmentation was manually corrected using ImageJ software (NIH, USA, http://rsb.info.nih.gov/ij). The "Find Connected Regions" plugin allows identifying voxel clusters which we separated manually in the binary image. For the 3D reconstruction, 3D Voxel object models were generated by connecting 2D regions within the binary images along the z-axis. Total number of spines, spine density along the dendrite, and quantitative morphological descriptors were calculated from the 3D voxel models. For visualization, active contour models were used, as described earlier (Härtel *et al.,* 2007). Smallest bounding, or enclosing boxes, were calculated relative to the principal axis of the 3D voxel objects which were determined as described. Length, width, and height of the boxes were calculated in addition to additional descriptors such as entropy, elongation, and relative volume. Entropy (E) provides a measure of compactness and ranges from 0 to 1. It is calculated from the object's eigenvalues $\lambda1 > \lambda2 > \lambda3$ from: $E = -1/\log(3) * \Sigma\, pi \log(pi)$, $pi = \lambda i / (\lambda1+\lambda2+\lambda3)$. Elongation (EL) ranges from 0 to 1 (minimum to maximum elongation) and was calculated by $EL = 1 - \lambda2/\lambda1$. Relative volume (RV) is calculated from RV = object volume / box volume, box volume = box length * box width * box height. Visualization and calculation of parameters was performed by image processing routines developed in SCIAN-Lab on the basis of interactive data language (IDL, Exelisvis). Spine shapes were defined using the morphological descriptors as follows i) Filopodia (F): length >=1.5 µm and Entropy <0.91, ii) Mushroom (M): <1.5 µm in length and >0.45 µm in width, iii) Stubby (S): <1.5 µm in length, >0.45 relative volume (RV), and <0.5 µm in elongation (EL), iv) Thin (T): <1.5 µm length and <0.45 in width or <1.5 µm in length and >0.5 in EL. Objects with ≤0.014 or > 0.2 in box volume (=box length x box width x box height) were excluded from the analysis since they were regarded either as unrelated to spine morphology or presented less of their volume within the slices selected for segmentation.

Novel Object Recognition (NOR) and Object Location Memory (OLM) tests. The NOR and OLM tasks were performed only with male mice at a specific time (morning) during the light cycle. The mice were handled for a week before testing. The single trail NOR and OLM tests consisted of 3 steps: habituation (3 trials on 3 consecutive days, 10 min/trial), a single 10 min duration training session, followed 24 hr later by a

10 min duration test session. For both behavioral tests, the mice were individually habituated in an apparatus that contained in a rectangular plastic cage of 30 cm × 30 cm x 40 cm (length×width×height), localized inside an insonorized chamber. In the training session, the cage contained 2 identical objects localized on the floor in the center of the cage; these objects are termed "familiar objects" in NOR and "none-displaced objects" in OLM. In the test session, mice were places again in the insonorized chamber with the following changes: In NOR, one familiar object (F) was replaced by a novel object (N), while in OLM, the location of one none-displaced object (none-D) was changed, termed displaced object (D). The exploration time was recorded and defined as time spent sniffing or touching the object with the nose and/or forepaws. For NOR, the "recognition index" was calculated by the time spent to explore object N compared to total time explored in both objects (N + F). For OLM, the "discrimination index" was calculated by the time spent to explore object D compared to total time explored in both objects (D + none-D). The cage and the objects were thoroughly cleaned between trials with 5% ethanol and air ventilated between tests.

Memory Flexibility (MF) test. The MF task was performed only with male mice at a specific time (morning) during the light cycle and as previously described (Serrano *et al.*, 2014) with slight modifications. The mice were handled for a week before beginning the test. A circular water maze of 1.3 m diameter was filled with opaque water at 50 cm deep (19–21°C). The mice were trained to find a circular platform of 10-cm localized at 1 cm below water level. Each animal was trained for one pseudo-random location of the platform per day for 4 days, with a new platform location each day. The maximum swimming trial duration was 60 s and animals were allowed to spend 10 s on the platform at the end of each trial. The delay time between trials was 10 to 15 min. Up to 15 training trials were performed per day or until the animal met a criterion of 3 successive trials within an escape latency of <20 s. Upon testing completion, the mouse was removed gently from the maze and returned to its cage. The latency to reach the platform and the trials to get the criterion was recorded with a video camera over the swim pool. Of note is that when the MF was performed with 12 mo AβPPswe/PS-1, three of twelve injected mice were discarded from the test because of the following reasons: One mouse (AAV-PSD95-6ZF-VP64 injected) died at 10.5 mo; one mouse (AAV-GFP injected) suffered a heart attack at the beginning of the MF test; one mouse (AAV-PSD95-6ZF-VP64 injected) showed severe locomotion dysfunction at 11.5 mo.

Electrophysiology. Slice preparation and electrophysiological recordings were performed as previously described (Fuenzalida *et al.*, 2007; Vargas *et al.*, 2014). Briefly, 3-4 days after HSV infections, mice were decapitated, and the brain was immediately removed and submerged in cold (~4°C) artificial CSF (ACSF; in mM: 124 NaCl, 2.69 KCl, 1.25 KH2PO4, 2 Mg2SO4, 26 NaHCO3, 2.5 CaCl2 and 10 glucose). The pH was stabilized at 7.4 by bubbling the ACSF with carbogen (95% O2, 5% CO2). Transverse hippocampal slices (250 µm thick) were cut with a Vibroslice microtome (VSL, WPI, Sarasota, FL) and incubated in ACSF (1 h, at room temperature, 20–22°C). The slices were transferred to a 2 ml chamber fixed to an upright microscope (FN1, Nikon). The slices were super-fused with carbogen-bubbled ACSF (2 ml/min) and maintained at room temperature. All recordings were made with picrotoxin (50 µM, Tocris) in the ACSF perfusion media to suppress GABAergic inhibitory transmission. Single cell recordings were made in the whole-cell configuration with fire-polished pipettes (3–5 MΩ) filled with intracellular solution (see below), connected to an EPC-7 patch-clamp amplifier (Heka Instruments), filtered at 3.0 kHz, sampled at 4.0 kHz using an A/D converter (ITC-16, InstruTech), and stored with Pulse FIT software (Heka Instruments). Single-electrode voltage-clamp recordings were obtained from dentate granular cells. In the voltage-clamp configuration, the series resistance was compensated to ~70%, and recordings were accepted only when the seal resistance was ~1GΩ and the series resistance (7–14 MΩ) did not change ~10% during the experiment. To improve the voltage-clamp conditions, the experiments were performed in a Cs-based intracellular solution containing in mM: 100 Cs-Gluconate, 10 HEPES, 10 EGTA, 4 Na2-ATP, 10 TEA-Cl and 1 MgCl2-6H2O, buffered to pH 7.2–7.3 with CsOH. The experiments started after a 5–10 min stabilization period following entry into the intracellular compartment with the patch electrodes. The voltage-clamp recordings were rejected when the access resistance (7–15 MΩ) increased 20% during the experiment. The evoked EPSC was elicited by bipolar cathodic stimulation connected an isolation unit (Isoflex, A.M.P.I.). Concentric electrodes (platinum/iridium, FHC Inc.) were placed at the middle third of the molecular layer to stimulate MPP inputs. Voltage-clamp data were high- pass filtered at 3.0 kHz and sampled at rates between 6.0 and 10.0 kHz through a Digidata 1322A (Molecular Devices). The measurement of the NMDA/AMPAR ratio was performed similarly as previously described (Myme *et al.*, 2003; Ehrlich *et al.*, 2007). The time of the peak current at -70 mV, considered to be completely mediated by AMPARs, was used to establish the window for measuring the AMPA-mediated eEPSC peak at +40 mV. To determine the NMDAR-EPSCs, the late +40 mV EPSC component was measured at 80-85 msec after stimulus. The paired pulse ratio (PPR) was calculated as (R2/R1) X 100, where R1 and R2 are the peak amplitudes of the first and second EPSCs, respectively. Sixty traces (5-min recording) were digitally averaged for calculations.

Dendritic arbor analysis *in vitro*. Fluorescently labeled hippocampal neurons in cultures were fixed in 4% paraformaldehyde and visualized on a confocal (Olympus FV 1000, Tokyo, Japan) or epi-fluorescence (Nikon eclipse Ti, Tokyo, Japan) microscope. The number of dendrites was counted and the length of each dendrite assessed with use of the semi-automated Metamorph software (Universal Imaging) as described (Sepulveda *et al.*, 2010; Henriquez *et al.*, 2013; Bustos *et al.*, 2014). Briefly, images were contrast-enhanced to ensure that we had analyzed all branches. The length of individual dendrites was measured by digitally marking every branch segment arising from the soma, from the origin of the branch to its termination. The investigator was blinded to the experimental conditions, to reduce researcher bias. Sholl analysis was performed with ImageJ (NIH), using a special plug-in designed by the Ghosh laboratory (available at www- biology.ucsd.edu/labs/ghosh/software/index.html).

Supplemental References

Ampuero E, Jury N, Härtel S, Marzolo M-P, van Zundert B. Interfering of the Reelin/ApoER2/PSD95 Signaling Axis Reactivates Dendritogenesis of Mature Hippocampal Neurons. J. Cell. Physiol. 2017; 232: 1187–1199.

Beltran A, Parikh S, Liu Y, Cuevas BD, Johnson GL, Futscher BW, et al. Re-activation of a dormant tumor suppressor gene maspin by designed transcription factors. Oncogene 2007; 26: 2791–2798.

Broekman MLD, Comer LA, Hyman BT, Sena-Esteves M. Adeno-associated virus vectors serotyped with AAV8 capsid are more efficient than AAV-1 or -2 serotypes for widespread gene delivery to the neonatal mouse brain. Neuroscience 2006; 138: 501–510.

Bustos FJ, Jury N, Martinez P, Ampuero E, Campos M, Abarzúa S, et al. NMDA receptor subunit composition controls dendritogenesis of hippocampal neurons through CAMKII, CREB-P, and H3K27ac. J. Cell. Physiol. 2017; 27: 8334.

Bustos FJ, Varela-Nallar L, Campos M, Henriquez B, Phillips M, Opazo C, et al. PSD95 suppresses dendritic arbor development in mature hippocampal neurons by occluding the clustering of NR2B-NMDA receptors. PLoS ONE 2014; 9: e94037.

Deverman BE, Pravdo PL, Simpson BP, Kumar SR, Chan KY, Banerjee A, et al. Cre-dependent selection yields AAV variants for widespread gene transfer to the adult brain. Nat Biotechnol 2016; 34: 204–209.

Falahi F, Huisman C, Kazemier HG, van der Vlies P, Kok K, Hospers GAP, et al. Towards Sustained Silencing of HER2/neu in Cancer By Epigenetic Editing. Molecular Cancer Research 2013; 11: 1029–1039.

Fuenzalida M, Fernandez de Sevilla D, Buno W. Changes of the EPSP Waveform Regulate the Temporal Window for Spike-Timing-Dependent Plasticity. Journal of Neuroscience 2007; 27: 11940–11948.

Härtel K, Singaravelu K, Kaiser M, Neusch C, Hülsmann S, Deitmer JW. Calcium influx mediated by the inwardly rectifying K+ channel Kir4.1 (KCNJ10) at low external K+ concentration. Cell Calcium 2007; 42: 271–280.

Henriquez B, Bustos FJ, Aguilar R, Becerra A, Simon F, Montecino M, et al. Ezh1 and Ezh2 differentially regulate PSD-95 gene transcription in developing hippocampal neurons. Mol. Cell. Neurosci. 2013; 57: 130–143.

Huisman C, Wisman GBA, Kazemier HG, van Vugt MATM, van der Zee AGJ, Schuuring E, et al. Functional validation of putative tumor suppressor gene C13ORF18 in cervical cancer by Artificial Transcription Factors. Mol Oncol 2013; 7: 669–679.

Kilkenny C, Browne WJ, Cuthill IC, Emerson M, Altman DG. Improving bioscience research reporting: the ARRIVE guidelines for reporting animal research. PLoS Biol. 2010; 8: e1000412.

Langmead B, Salzberg SL. Fast gapped-read alignment with Bowtie 2. Nature Methods 2012; 9: 357–359.

Mandell JG, Barbas CF. Zinc Finger Tools: custom DNA-binding domains for transcription factors and nucleases. Nucleic Acids Research 2006; 34: W516–23.

Myme CIO, Sugino K, Turrigiano GG, Nelson SB. The NMDA-to-AMPA ratio at synapses onto layer 2/3 pyramidal neurons is conserved across prefrontal and visual cortices. Journal of Neurophysiology 2003; 90: 771–779.

Neve RL, Neve KA, Nestler EJ, Carlezon WA. Use of herpes virus amplicon vectors to study brain disorders. Biotech. 2005; 39: 381–391.

Sepulveda FJ, Bustos FJ, Inostroza E, Zuniga FA, Neve RL, Montecino M, et al. Differential Roles of NMDA Receptor Subtypes NR2A and NR2B in Dendritic Branch Development and Requirement of RasGRF1. Journal of Neurophysiology 2010; 103: 1758–1770.

Serrano FG, Tapia-Rojas C, Carvajal FJ, Hancke J, Cerpa W, Inestrosa NC. Andrographolide reduces cognitive impairment in young and mature AβPPswe/PS-1 mice. Mol Neurodegeneration 2014; 9: 61.

Tashiro A, Sandler VM, Toni N, Zhao C, Gage FH. NMDA-receptor-mediated, cell-specific integration of new neurons in adult dentate gyrus. Nature 2006; 442: 929–933.

Vargas JY, Fuenzalida M, Inestrosa NC. In vivo Activation of Wnt Signaling Pathway Enhances Cognitive Function of Adult Mice and Reverses Cognitive Deficits in an Alzheimer's Disease Model. Journal of Neuroscience 2014; 34: 2191–2202.

Wyneken U, Smalla KH, Marengo JJ, Soto D, la Cerda de A, Tischmeyer W, et al. Kainate-induced seizures alter protein composition and N-methyl-D-aspartate receptor function of rat forebrain postsynaptic densities. Neuroscience 2001; 102: 65–74.